Alpine exhumation of the central Cantabrian Mountains, Northwest Spain

C. Fillon[1,2], D. Pedreira[3], P. A. van der Beek[1], R. S. Huismans[4], L. Barbero[5], and J. A. Pulgar[3]

[1]ISTerre, Université Grenoble Alpes, CNRS, Grenoble cedex, France, [2]GET, Observatoire Midi Pyrénées, Université de Toulouse, CNRS, IRD, Toulouse, France, [3]Departamento de geología, Universidad de Oviedo, Oviedo, Spain, [4]Department of Earth Sciences, Bergen University, Bergen, Norway, [5]Departamento de Ciencias de la Tierra, Facultad de Ciencias del Mar y Ambientales, Universidad de Cadiz, Cadiz, Spain

Abstract The Cantabrian Mountains extend along the Atlantic coast of northern Spain and are known to have experienced an Alpine phase of deformation, reactivating well-expressed Variscan structures. They form the westward continuation of the Pyrenean range and were similarly uplifted consequently to the convergence between the Iberian and European plates. Nevertheless, due to the scarcity of syntectonic sediments and structural markers in a large outcrop of Variscan basement, little is known about the precise timing and amount of the Alpine exhumation phase in the Cantabrian Mountains. We present a new low-temperature thermochronology data set, composed of nine apatite fission track (AFT) and six zircon (U-Th)/He (ZHe) ages, sampled along structurally well-constrained N-S profiles through the central part of the Cantabrian Mountains and complemented by 3-D thermokinematic modeling. The occurrence of Eocene-Oligocene AFT and ZHe ages in the center of the profiles allows us to frame the period of Alpine exhumation from 39 to 29 Ma, at a rate of 0.24–0.3 km Myr^{-1}. Moreover, the reset ZHe ages imply significant burial of the samples, by up to 8–10 km in the center of the range. Therefore, the Alpine exhumation phase was significant, and synchronous to the main phase of exhumation in the central Pyrenees, although exhumation rates were an order of magnitude lower. Three-dimensional thermokinematic modeling of the data confirms the timing of uplift of this area, but its resolution is limited by the relatively small number of reset ages over a large area.

1. Introduction

Pyrenean deformation linked to convergence between the Iberian and European plates is widespread along northern Spain and implies contraction in the Pyrenees, the Basque-Cantabrian basin, and the Cantabrian mountains during Eocene to Miocene times. Although numerous studies have addressed the timing and spatial pattern of exhumation in the Pyrenean range [e.g., *Fitzgerald et al.*, 1999; *Gibson et al.*, 2007; *Jolivet et al.*, 2007; *Maurel et al.*, 2007; *Metcalf et al.*, 2009; *Morris et al.*, 1998; *Sinclair et al.*, 2005; *Yelland*, 1990], very little is known on that subject in the Cantabrian Mountains. The earlier Variscan deformation phase has been much less overprinted by Cenozoic deformation in the Cantabrians than in the Pyrenees, and the scarcity of Mesozoic outcrops in the central and western parts of this range makes difficult the quantification of the Alpine deformation. Moreover, the lack of appropriate rocks for thermochronological analyses has rendered the isolation of Alpine exhumation patterns tricky [e.g., *Carrière*, 2006; *Grobe et al.*, 2010; *Martin-Gonzalez et al.*, 2011]. Similarly, timing estimates for activity on the frontal thrusts are provided by continental deposits that are well preserved and precisely dated in front of most of the Pyrenees but poorly dated in the Cantabrian area. Final activity on the frontal thrusts was dated to Chattian times (26–28 Ma) in the eastern [*Vergés et al.*, 2002; *Vergés et al.*, 1995], central [*Meigs et al.*, 1996], and western Pyrenees [*Teixell*, 1998]. In the Cantabrian Mountains, activity on the frontal thrust has been estimated to be more recent, even though the dating of the foreland sediments of the Duero basin is less precise [*Alonso et al.*, 1996]. There are, however, good floral and faunal paleontological ages in the Oviedo piggyback basin, located in the northern flank of the Cantabrian Mountains (Figure 2), where continental deposits near the base of the Tertiary succession yielded Bartonian-Priabonian ages (41–34 Ma) [*Casanovas-Cladellas et al.*, 1991; *Truyols and García Ramos*, 1991]. Between the Cantabrian Mountains and the Pyrenees, there is some evidence of Alpine contractional structures affecting Early Miocene sediments in the Basque-Cantabrian basin, therefore dating the most recent activity. On the other hand, published thermochronological ages for samples collected in the western Cantabrians [*Carrière*, 2006; *Grobe et al.*, 2010; *Martin-Gonzalez et al.*, 2011] do not show evidence of

significant Alpine exhumation to the west of our study area. Published apatite fission track (AFT) ages range from Triassic to Late Cretaceous, and there is a lack of data in the central Cantabrians, where Alpine shortening is supposed to be maximum [*Pulgar et al.*, 1999]; only two AFT samples have yielded Oligocene ages in this area [*Carrière*, 2006].

In this study, we use low-temperature thermochronology data to constrain both the timing and pattern of Alpine exhumation in the central Cantabrian Mountains, which is also the area of highest elevation and relief (*Picos de Europa* area). This study aims to unravel the Alpine history by dating more precisely the main episode of deformation as well as quantifying the amount of exhumation, placing these results in the context of the whole Pyrenean-Cantabrian orogenic system. To that purpose, we introduce in the following apatite fission track ages and track lengths, together with (U-Th)/He analyses on zircons. Thermal-kinematic inverse modeling [*Braun et al.*, 2012] is also presented to quantitatively analyze the data in terms of the structure and kinematics of the central Cantabrian Mountains. Our data provide important new constraints on the timing and amount of Alpine exhumation in this region but have limited resolution in detailing the precise structure and kinematics of the range.

2. Geological Background

The Cantabrian Mountains extend to the west up to the Atlantic Ocean and are bounded by the Bay of Biscay to the North and the Duero foreland basin to the south (see Figure 1a). They represent the western continuation of the Pyrenean orogen and result from the collision of the Iberian plate with the European plate. To the east, the Iberian plate has underthrusted the European plate to build the Pyrenees [*Choukroune and ECORS Team*, 1989; *Muñoz*, 1992; *Pedreira et al.*, 2003; *Teixell*, 1998; *Vergés et al.*, 1995; *Mouthereau et al.*, 2014]. To the west, the Cantabrian Mountains reflect inversion of the North-Iberian margin and the Mesozoic Basque-Cantabrian basin, rather than a full continental collision [*Gallastegui*, 2000; *Pedreira et al.*, 2003; *Pedreira et al.*, 2007, 2015; *Roca et al.*, 2011]. Shortening by margin inversion was concentrated within the Iberian plate itself, with the development of a prominent crustal root by north directed crustal underthrusting [*Fernández-Viejo et al.*, 1998; *Gallastegui*, 2000; *Pedreira et al.*, 2003; *Pulgar et al.*, 1996]. Note that in the following the denominations "eastern Cantabrians" and "central Cantabrians" are used, respectively, for the Basque-Cantabrian basin and the area along the ESCIN-2 profile (see black box in Figure 1).

2.1. Structural Inheritance

To understand the Cenozoic deformation of the Cantabrian Mountains, one needs to take into account that this area experienced a long-term deformation history, including the Variscan orogeny, followed by two phases of Mesozoic extension and finally the Alpine phase of contractional deformation. The Variscan orogeny, which affected the Cantabrian Mountains area during the Carboniferous, had a major impact on the structure of the belt (Figure 1a). The Cantabrian Zone represents the external part of the Variscan belt: it was shaped by a thin-skinned imbricate thrust structure progressing from west to east (Figure 1a) [*Julivert*, 1971; *Pérez-Estaùn et al.*, 1988]. The Variscan basement and its internal basins are unconformably overlain by Stephanian sediments that date the end of this orogenic phase at around 305 Ma. However, all these units were subsequently deformed by a N-S shortening event around the Carboniferous-Permian boundary that resulted in oroclinal bending and the formation of the so-called "Asturian Arc" or "Cantabrian Orocline" [e.g., *Weil et al.*, 2013]. Most of the large structures observed today were formed during these two phases, which resulted in major east-west trending thrusts in the eastern and central parts of the range and north-south trending arcuate faults to the west (e.g., Figure 1a). Some of the east-west trending faults in the eastern part of the Cantabrian Zone were reactivated during the subsequent phase of Mesozoic extension as well as during the Alpine convergence phase [*Alonso et al.*, 1996; *Pulgar et al.*, 1999].

The first Mesozoic extensional episode started during Permian and Triassic times [*Espina et al.*, 2004; *Lepvrier and Martinez-Garcia*, 1990]; and a second phase affected the area from the Late Jurassic to the Early Cretaceous, leading to the opening of the Bay of Biscay [*Olivet*, 1996; *Pujalte et al.*, 2004]. Extension peaked during Aptian-Albian times, with development and reactivation of E-W faults that define horst-and-graben systems, mostly in the present-day eastern Cantabrian Mountains (the Basque-Cantabrian basin). In the central Cantabrian Mountains, Cretaceous synrift sediments are present along the coastline and especially in the offshore Le Danois basin [*Ferrer et al.*, 2008; *Roca et al.*, 2011]. The Mesozoic basins experienced a phase of postrift subsidence before the Cenozoic reactivation of the structures. However, this was discrete in the present-day
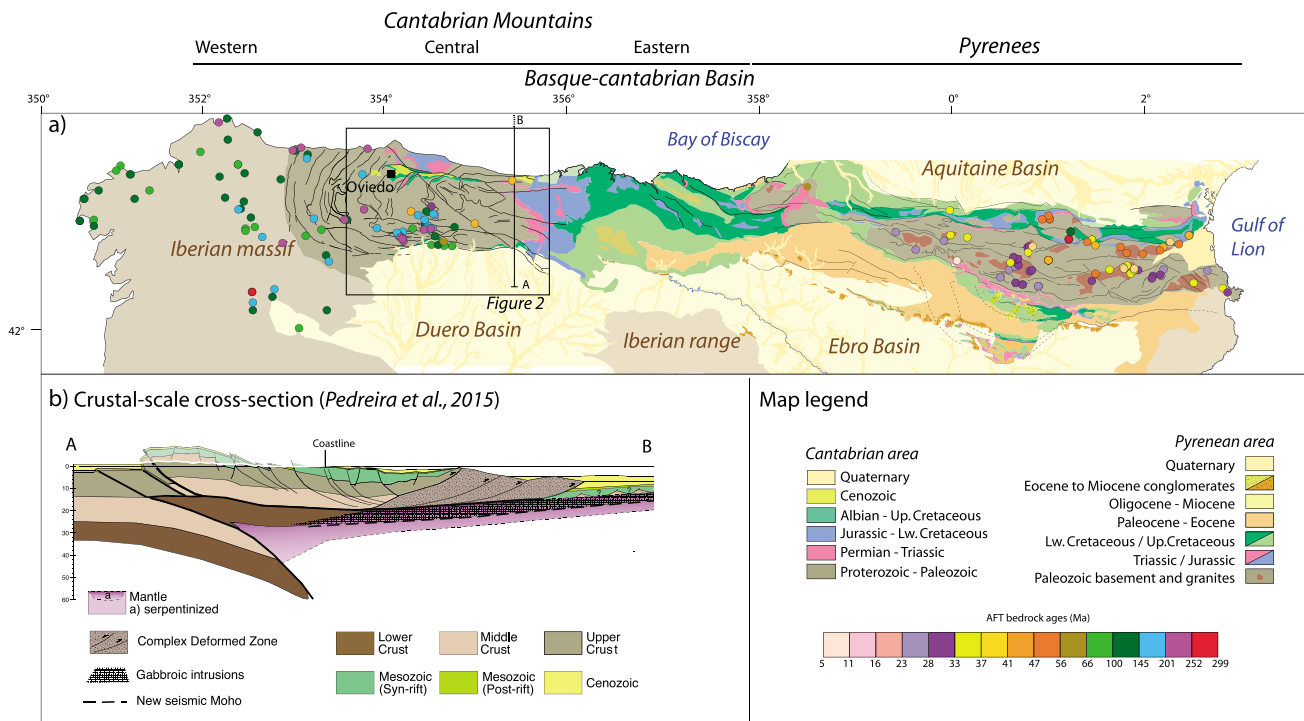
Figure 1. (a) Overview map of the Pyrenean-Cantabrian system, including AFT bedrock ages from *Yelland* [1990], *Morris et al.* [1998], *Fitzgerald et al.* [1999], *Sinclair et al.* [2005], *Carrière* [2006], *Gibson et al.* [2007], *Jolivet et al.* [2007], *Maurel et al.* [2007], *Gunnel et al.* [2009], *Metcalf et al.* [2009], *Grobe et al.* [2010], *Martin-Gonzalez et al.* [2011], and *Botor and Anczkiewicz* [2015]. Inset shows location of Figure 2. (b) Crustal-scale cross section across the central Cantabrian Mountains and offshore margin, showing Alpine deformation structures, modified from *Pedreira et al.* [2015]. Note that the cross section continues further North, out of the map drawn here.

central Cantabrian Mountains, as recorded by coastal and shallow marine sediments with a total thickness not exceeding a few hundreds of meters [*Gallastegui*, 2000; *Herrero-Hernández and Gómez-Fernández*, 2012; *Pulgar et al.*, 1999].

2.2. Alpine Deformation in the Central Cantabrians

The central Cantabrians are spatially located over the Variscan Cantabrian Zone (Figures 1 and 2), between the inverted Basque-Cantabrian basin (Eastern Cantabrians) and the western outcrops of the Variscan Iberian massif, where the Alpine relief and deformation is less pronounced (western Cantabrians) [*Barnolas and Pujalte*, 2004]. The Alpine phase of N-S contractional deformation initiated in the North-Iberian (or Cantabrian) margin during Eocene times with inversion of extensional structures to form a north vergent accretionary wedge at the former continental slope (Figure 1b) [*Alvarez-Marron et al.*, 1997; *Boillot et al.*, 1979; *Fernández-Viejo et al.*, 2012; *Gallastegui et al.*, 2002; *Roca et al.*, 2011]. Dating of this phase is constrained by offshore syntectonic sediments that are Late Eocene in age [*Alonso et al.*, 1996; *Alvarez-Marron et al.*, 1997; *Gallastegui*, 2000]. The previous (Mesozoic) continental platform and coastal areas were at this stage affected by south verging structures, the most significant of which is the frontal thrust over the Duero foreland basin. The end of N-S contraction can be extrapolated from the age of the uppermost syntectonic strata at the northern edge of the Duero basin. The absolute age of the Paleogene-Neogene syntectonic sediments still lacks precision due to their continental depositional environment, which renders biostratigraphic dating of these rocks difficult. Nevertheless, activity on the frontal thrust of the central Cantabrian Mountains is bounded by the age of essentially posttectonic conglomeratic deposits sealing the syntectonic sediments, which are Late Miocene (Vallesian-Turolian) in age [*Herrero et al.*, 2010, and references therein]. N-S contraction is thus inferred to have affected the Cantabrian Mountains from middle Eocene until lower Miocene times.

Based on geological field observations, *Alonso et al.* [1996] and *Pulgar et al.* [1999] interpreted the structure of the central Cantabrian Mountains as a crustal-scale fault bend fold accommodated by a major ramp that
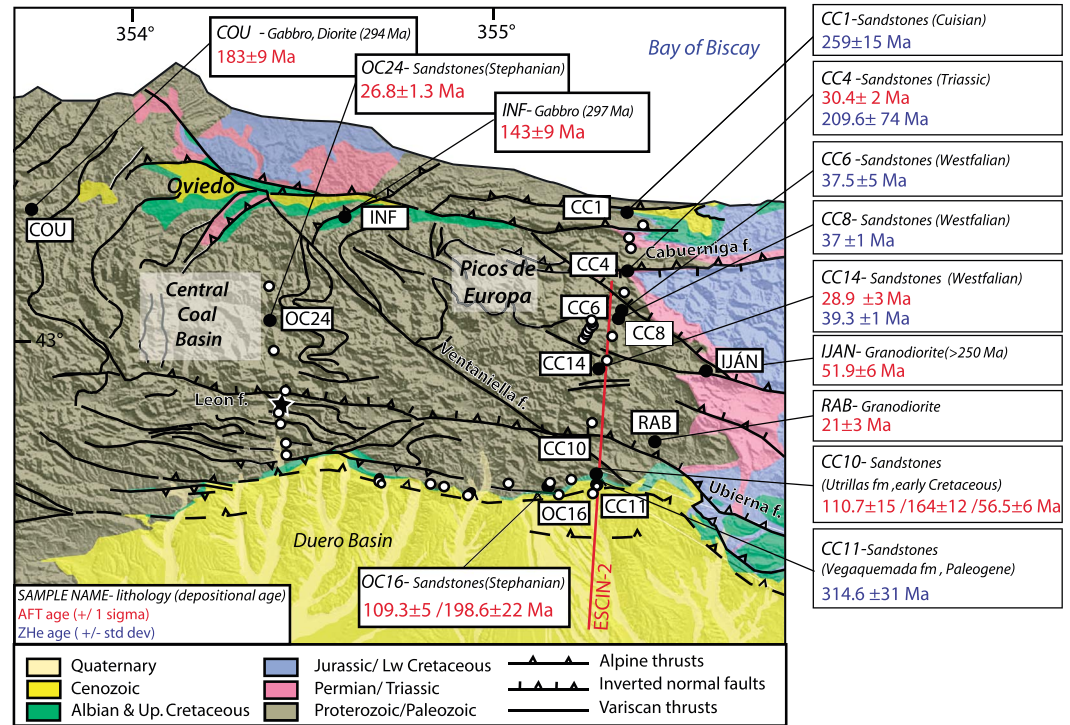
Figure 2. Sampling sites and new AFT and ZHe ages plotted on the geological map. Open circles represent samples that did not yield sufficient apatite or zircon for analyses, filled circles with sample codes represent samples for which ZHe ages (in blue) and/or AFT ages (in red) were determined. AFT age distribution for samples OC16 and CC10 have multiple age populations; all are indicated with the first age representing the main age peak (see Figure 3 for details). The white star is the location of the sample yielding an Oligocene AFT age in *Carrière* [2006], plotted in Figure 4.

roots at 15–20 km depth and emerges at the southern front of the belt (Figure 4). From the dip of the Mesozoic layers in the dorsal culmination [*Butler*, 1982], the authors extrapolated a ramp angle of ~15° toward the north, later reassessed up to 18° [*Pulgar et al.*, 1999, Figure 4]. All other Alpine thrusts that emerge at the surface are north dipping. They are easily identified in the northern and southern flanks of the mountain belt, where they offset Mesozoic sediments, and in many cases they show up as reactivations of E-W trending Variscan thrusts. The deformation is of thick-skinned style, with the cover and the basement deforming jointly during the Alpine deformation [*Alonso et al.*, 1996; *Pulgar et al.*, 1999]. Within the central part of the range, where the Mesozoic cover has been eroded away, it is more difficult to recognize Alpine deformation in the basement. The displacement accommodated by the main crustal thrust emerging at the mountain front was estimated to be of ~25 km from structural reconstructions [*Alonso et al.*, 1996; *Pulgar et al.*, 1999], but total shortening increases up to ~96–98 km when the crustal-scale deformation, including the north verging wedge, is taken into account [*Gallastegui*, 2000; *Pedreira et al.*, 2015].

2.3. Tectonic Continuity From the Pyrenees to the Cantabrian Mountains

The continuity of northward underthrusting of the Iberian crust from the Pyrenees to the Cantabrians has been demonstrated by numerous deep seismic reflection profiles, such as Etude Continentale et Océanique par Reflexion et Refraction Sismique in the Pyrenees [*ECORS Pyrenees Team*, 1988] and Seismic Study of the North Iberian Crust (ESCIN) in the Cantabrian mountains area [*Pulgar et al.*, 1997]. Geological mapping and several geophysical studies have imaged the southern Pyrenean contractional front continuing westward until the western Cantabrian mountains, where the front line rotates toward the north [e.g., *Martin-Gonzalez and Heredia*, 2011]. Moreover, the ESCIN deep seismic reflection profiles and associated refraction/wide-angle reflection surveys have permitted imaging the deep structure of the Cantabrian Mountains and adjacent Bay of Biscay margin in some detail [*Alvarez-Marron et al.*, 1996; *Fernández-Viejo et al.*, 2000, 1998;

Gallastegui, 2000; *Pedreira et al.*, 2003; *Pulgar et al.*, 1996; *Roca et al.*, 2011]. The most common interpretation is that north verging underthrusting of the Iberian lower crust and mantle, well established beneath the Pyrenees and the central Cantabrian Mountains, is a continuous feature in between these two regions, and beneath the Basque-Cantabrian basin, as suggested by a 3-D modeling of gravity and seismic data [*Pedreira et al.*, 2003, 2007]. These authors also concluded that the style of contractional deformation between the Pyrenees and the Cantabrian Mountains is partitioned by large N-S to NE-SW transverse structures in the Basque-Cantabrian basin.

2.4. The Duero Foreland Basin

The Duero basin is a large intracontinental basin that drains several mountain ranges surrounding it: the Iberian Range to the east, the Cantabrian Mountains to the north, and the Central System to the south (Figure 1a). To the west, it unconformably overlies the Variscan Iberian Massif. The Northern part of the basin has been filled by ~2.5 km of Paleogene to Miocene deposits, most of which were sourced from the Cantabrian Mountains. Alpine loading within the Cantabrian Mountains led to flexural isostatic subsidence of around 1.5 km [*Alonso et al.*, 1996] and the present-day elevation of the basin is ~1000 m at its northern border and ~845 m on average [see *Casas-Sainz and De Vincente*, 2009]. This high elevation and widespread preservation of sediments are due to the fact that the basin was endorheic during much of the Cenozoic and is affected by a semiarid and little erosive climate. At the Cantabrian Mountain front, the Oligocene-early Miocene infilling of the basin was perturbed by the development of a fault propagation fold at the tip of the crustal ramp discussed above. This deformation is especially clear in the eastern part of the central Cantabrians (along the ESCIN-2 section Figure 2), where the frontal conglomeratic deposits show spectacular growth strata geometries, including inverted layers [*Alonso et al.*, 1996].

3. Methodology

3.1. Sampling Sites

Our initial strategy was to collect samples in the area of highest elevations within the Cantabrian Mountains, excluding the Picos de Europa massif, which is almost exclusively composed of Carboniferous massive limestones. We collected and prepared 53 samples concentrated on three profiles (see white and black dots in Figure 2): (1) 23 samples along the trace of the ESCIN-2 seismic profile, from the Atlantic coast to the Duero basin, which also corresponds to one of the crustal cross sections presented by *Alonso et al.* [1996] and *Pulgar et al.* [1999]. Here we sampled sedimentary units of the Pisuerga-Carrión Province within the Variscan Cantabrian Zone, as well as some Mesozoic sandstones in the western termination of the Basque-Cantabrian basin; (2) 8 samples along another north-south profile, ~75 km to the west, following the other cross section proposed by *Alonso et al.* [1996] and *Pulgar et al.* [1999], across the Central Coal Basin of the Cantabrian Zone (Westphalian and Stephanian sandstones); and (3) 22 samples along an E-W profile along the southern mountain front and the northern limit of the Duero basin. Sampling was focused on siliciclastic units (Stephanian sandstones, Cretaceous Utrillas formation, and Paleogene Vegaquemada formation) along short N-S sections [see *Pulgar et al.*, 1999, Figure 3] crossing the mountain front. There, we expected to characterize the main exhumation phase along the front and to compare it to the record of the synorogenic sediments deposition in the most proximal part of the basin.

Of these 53 samples (black and white dots in Figure 2), only five produced sufficient apatite for fission track analysis, although most samples yielded sufficient high-quality zircon for (U-Th)/He dating; six of them were selected for dating (black dots in Figure 2a represent samples successfully analyzed by either of these two techniques). We combine these data with four samples from small intrusive bodies throughout the Cantabrian Mountains, collected and analyzed separately by L. Barbero (COU, INF, RAB, and IJAN). Thus, in total, we present nine AFT and six zircon (U-Th)/He (ZHe) results. Lithologies, stratigraphic ages, and coordinates for all the studied samples are listed in Table 1. The most suitable lithologies were found to be the Santonian turbidites, even though no sample yielded more than 40 grains of apatite. Other lithologies did not contain apatite at all and even the intrusive rocks contained very few apatite grains.

3.2. Apatite Fission Track Analysis

For this study, apatite grains were separated from granodiorite and fine- to medium-grained sandstone samples using conventional heavy liquid and magnetic separation techniques. Apatite aliquots were mounted in epoxy,

Table 1. Apatite Fission Track Results for the Cantabrian Mountains[a]

Sample	Stratigraphic/ Crystalization Age	Lat (°N)	Lon (°E)	Elevation (m)	No Grains	ρ_s (Ns) 10^5 cm^{-2}	ρ_i (Ni) 10^5 cm^{-2}	ρ_d (Nd) 10^5 cm^{-2}	$P(\chi^2)$ (%)	Age Dispersion	Central Age ($\pm1\sigma$, Ma)	MTL ($\pm1\sigma$, μm)	No Tracks	SD (μm)	Dpar (μm)
						Sedimentary Samples									
CC4	Triassic (220 Ma)	43.253	−4.581	421	20	6.662 (888)	14.292 (1905)	5.51 (4192)	18.8	0.11	30.4 ± 2.1				
CC14	Stephanian (300 Ma)	43.045	−4.652	1125	14	3.81 (197)	8.664 (448)	5.522 (4192)	56.9	0.02	28.9 ± 2.9				
OC16	Stephanian (300 Ma)	42.794	−4.784	1116	35	16.36(2388)	8.6022 (1256)	6.44 (4262)	≪1	0.24	128.8 ± 7.7	9.0 ± 0.4	26	2.0	1.3
CC10	Albian (110 Ma)	42.832	−4.651	1203	29	21.11 (3509)	11.142 (1852)	5.515 (4292)	≪1	0.29	124.5 ± 10.0	10.1 ± 0.4	31	2.0	1.4
OC24	Stephanian (300 Ma)	43.126	−5.565	528	41	5.354 (1182)	13.099 (2892)	6.467 (4262)	13.2	0.12	26.8 ± 1.3	11.2 ± 0.8	12	2.7	1.8
						Igneous Samples									
UAN	Pre-Triassic > 250 Ma	43.052	−4.337	2083	12	3.124(149)	12.015(573)	12.1(3768)	≪1	0,23	51.9 ± 6.1				
COU	Permian (294 Ma)	43.332	−6.245	700	17	0.688 (76)	6.312 (697)	11 (3482)	32,88	0,05	183.4 ± 9				
INF	Permian (297 Ma)	43.329	−5.353	310	10	5.6 (447)	7.542 (602)	11.5 (3487)	52,44	0,01	143.1 ± 9.5	12.1 ± 0.3	22	1.3	2.0
RAB	Pre-Triassic > 250 Ma	42.887	−4.48	1080	15	12.794(1131)	12.80(1132)	11.5 (3487)	41,18	0,06	21.3 ± 2.6				2.0

[a]The data were produced by L. Barbero and C. Fillon and merged together for consistency; LB sampled and analyzed sedimentary samples for AFT and ZHe dating; CF sampled and analyzed plutonic samples for AFT dating; CF sampled and analyzed sedimentary samples for AFT and ZHe dating. ρ_s and ρ_i are the measured spontaneous and induced track densities; ρ_d is the induced track density in the dosimeter glass, in brackets are the number of tracks counted; $P(\chi^2)$ is the χ^2 probability that the data represent a single age population; $P(\chi^2) \ll 1$ and/or an age dispersion >15% indicates that the age distribution has multiple populations; MTL is the measured mean track length, with SD its standard deviation; Dpar is the average etch pit width. Zeta values are 217 ± 3 for CF and 337 ± 5 for LB.

polished to expose internal crystal surfaces, and etched with 5.5 M HNO_3 for 20 s at 21°C for the sedimentary samples analyzed by CF (Charlotte Fillon) and 5 M HNO3 for 20 ± 1 s at 20 ± 0.5°C for the intrusive samples analyzed by LB (Luis Barbero). Low-U muscovite sheets were fixed to the mounts, to be used as external detectors, and then samples were sent for irradiation in the FRM II Research Reactor at the Technische Universität München (Germany). Apatite samples were irradiated together with IRMM 540R dosimeter glasses and Durango and Fish Canyon Tuff age standards. After irradiation the mica sheets of sedimentary samples and standards were etched in 48% HF for 18 min at 21°C (CF) and 40 min at room temperatures for granodiorite samples (LB). The samples and standards were counted dry at 1250 magnification, using an Olympus BH2 optical microscope (CF) and a Zeiss Axio Imager M1 microscope with magnification of 1000X (LB), with the FTStage 4.04 system of *Dumitru* [1993]. Most samples yielded only few datable grains; as many grains as possible were counted for each sample.

Fission track ages were calculated using the zeta calibration method and the standard fission track age equation [*Hurford and Green*, 1983]. The χ^2 test and age dispersion [*Galbraith and Green*, 1990; *Galbraith and Laslett*, 1993] were used to assess the homogeneity of AFT ages. Two samples (CC10 and OC16) yielded dispersed ages incompatible with a single age component; the grain age distributions of these samples were decomposed into major grain age components or peaks using binomial peak fitting [*Stewart and Brandon*, 2004]. We were able to measure horizontal confined track lengths in three samples, using a digitizing tablet and drawing tube. The widths of tracks crossing the etched internal surface (Dpar) were measured using the same digitizing techniques as used for measuring track lengths.

3.3. (U-Th)/He Analyses on Zircon

Among the samples yielding sufficient zircons, six were selected for (U-Th)/He dating, according to the quality of the grains and their geographic distribution along the eastern cross section. Clear and undisturbed zircon grains without inclusions were selected using a binocular microscope. The grain dimensions were measured for calculation of the α correction factor F_t [*Farley et al.*, 1996]. Single grains were subsequently packed in Nb tubes for (U-Th)/He analysis. We analyzed three aliquots per sample in the Patterson helium extraction line at the University of Tübingen (Germany), which is equipped with a 960 nm diode laser to extract the helium gas. Zircon grains were heated for 10 min at 20 A. Each grain was heated and analyzed a second time to make sure that the grain was degassed entirely in the first step. The re-extracts generally released <1% of the amount of gas released during the first step. After helium analysis, the grain packages were sent to the University of Arizona at Tucson (USA) for U and Th measurements by inductively coupled plasma mass spectrometry. The analytical error of the mass spectrometer measurements is generally very low and does not exceed 2%. In contrast, the reproducibility of the sample age constitutes a much larger error. We therefore report the mean (U-Th)/He age and the standard deviation of the measured aliquots as the sample error.

4. Results

Results are reported in Tables 1–3 and plotted in Figures 2 and 3. In order to discuss the structural implications of these new data, the results are also projected on the structural cross section in Figure 4. Most of the samples that yielded results are located along the trace of the ESCIN-2 profile in the eastern part of the central Cantabrians. Only three samples with AFT data are located further west, in the Central Coal Basin, and will be presented independently.

4.1. Eastern Profile: The ESCIN-2 Section

Four of the samples along this profile are characterized by a single AFT grain age population (CC4, CC14, IJAN, and RAB), while two show multiple populations (CC10 and OC16; Figure 3 and Table 3). The ZHe ages presented in Figure 2 are the mean ages from the measurements on the three individual grains for each sample. These measurements are detailed in Table 2 and can be used to differentiate between two group of samples. A first one shows variable Paleozoic-Mesozoic single-grain ages (130–342 Ma) and are interpreted to be unreset with regard to the Cenozoic deformation (CC1, CC4, and CC11); a second group is characterized by young single-grain ages (34–45 Ma) and very good reproducibility between the grains (CC6, CC8, and CC14), interpreted as being fully reset. The reproducibility of the Cenozoic reset ages is consistent with the interpretation of these results as recording an orogenic cooling episode, whereas the unreset samples could be interpreted as recording more protracted cooling. Together, the AFT and ZHe data delimit three areas characterized by distinct age patterns along the ESCIN-2 transect (Figure 4):

Table 2. Zircon (U-Th)/He Results[a]

Sample	Stratigraphic Age	Lat (°N)	Lon (°E)	Elevation (m)	4-He (mol)	238-U (mol)	232-Th (mol)	Uncorr. Age (Ma)	F_t	Corrected Age (Ma)	Mean Age (Ma)	SD
CC1_A	Lw. Eocene	43.379	−4.592	34	1.776E-12	5.869E-12	1.369E-12	218.09	0.792	274.0		
CC1_B	(50 Ma)				1.583E-12	5.247E-12	2.210E-12	209.19	0.804	259.0		
CC1_C					3.263E-12	1.144E-11	4.658E-12	198.60	0.811	243.9	259.0	15.0
CC4_A	Triassic	43.253	−4.581	421	6.486E-13	2.105E-12	1.263E-12	206.16	0.743	275.8		
CC4_B	(220 Ma)				1.060E-12	4.449E-12	1.800E-12	166.50	0.742	223.3		
CC4_C					1.948E-12	1.259E-11	1.189E-11	97.82	0.752	129.7	209.6	74.0
CC6_A	Stephanian	43.170	−4.592	368	6.228E-13	1.262E-11	2.973E-12	36.15	0.809	44.6		
CC6_B	(300 Ma)				7.672E-14	1.825E-12	1.630E-12	26.99	0.788	34.2		
CC6_C					9.460E-14	1.889E-12	2.223E-12	30.50	0.749	40.7	37.5	4.6
CC8_A	Stephanian	43.152	−4.601	310	7.851E-14	2.055E-12	6.640E-13	27.48	0.720	38.1		
CC8_B	(300 Ma)				2.038E-13	5.278E-12	1.735E-12	27.75	0.740	37.5		
CC8_C					6.029E-13	1.504E-11	6.260E-12	28.27	0.798	35.4	37.0	1.4
CC14_A	Stephanian	43.045	−4.652	1125	7.151E-13	1.710E-11	2.595E-12	31.20	0.787	39.6		
CC14_B	(300 Ma)				4.326E-13	1.091E-11	2.131E-12	29.30	0.763	38.4		
CC14_C					1.257E-12	2.878E-11	1.003E-11	31.24	0.780	40.0	39.3	0.9
CC11_A	Eocene-Oligocene	42.814	−4.647	1118	2.984E-12	8.297E-12	1.420E-12	261.59	0.812	320.4		
CC11_B	(56–23 Ma)				2.044E-12	6.197E-12	2.664E-12	227.94	0.806	281.5		
CC11_C					1.394E-12	3.368E-12	2.546E-12	267.34	0.777	341.9	314.6	30.6

[a]F_t is the geometric correction factor for age calculation. He measurements were performed at the University of Tübingen (Germany) and U and Th measurements at the University of Arizona (USA). We use the mean age, which is the arithmetic mean of the three corrected single-grain ages and its standard deviation.

1. From the coastline to sample CC4, located to the south of the trace of the Cabuérniga Fault, the samples have reset Cenozoic AFT ages (CC4, 30.4 ± 2.1 Ma) associated with much older (Permian-Triassic) ZHe ages (CC1, 259 ± 15 Ma; CC4, 210 ± 74 Ma). Sample CC4 shows a significant spread in single-grain ZHe ages, between 130 and 276 Ma. Interestingly, this sample is located between a sample to the north with old (Permian-Triassic) ages and the group of samples with young ZHe ages to the south; it may thus record partial resetting of the ZHe system.

2. The second region groups samples from the center and south of the section and is characterized by Cenozoic resetting of both AFT and ZHe ages. In this area, the ZHe ages are very similar and associated with low uncertainties (ages of 37.5 ± 4.6, 37.0 ± 1.4 and 39.3 ± 0.9 Ma for samples CC6, CC8, and CC14, respectively). The combination of both young AFT (28.9 ± 2.9 Ma, CC14) and ZHe ages clearly indicates that this area experienced most exhumation during Alpine deformation. On the other hand, two additional samples collected from intrusive rocks to the east of the section (IJAN and RAB) show slightly different results, showing AFT ages of 51.9 ± 6.1 Ma (IJAN) and 21.3 ± 2.6 Ma (RAB). These results contrast with the homogeneity of the AFT and ZHe ages across the ESCIN-2 transect and could be linked to the change in structural pattern to the east, at the limit with the Basque-Cantabrian basin area. The implications of these results will be further discussed in the next section. In any case, these two Eocene-lower Miocene ages clearly reveal the Alpine resetting of this wide region.

3. Finally, the third set of data, located in the southernmost part of the cross section, south of the Ubierna Fault, is characterized by AFT ages with multiple populations (Table 3 and Figure 3) and a late Carboniferous (i.e., Variscan) ZHe age. Samples OC16 and CC10 (sandstones deposited, respectively, during Stephanian and Albian times) both have AFT age distributions with Albian peak ages (109 ± 5 Ma and 111 ± 5 Ma, respectively) and secondary Jurassic peak ages (199 ± 22 Ma and 164 ± 12 Ma). Sample CC10 additionally has a small early Cenozoic (57 ± 6 Ma) age peak. All these features clearly

Table 3. Details of AFT Results for Samples With Multiple Populations[a]

Sample	Stratigraphic Age (Ma)	P1 ± 1σ (Ma)	P2 ± 1σ (Ma)	P3 ± 1σ (Ma)
OC16	300		**109.3 ± 5.3 (79.4 %)**	198.6 ± 22.3 (20.6 %)
CC10	110	56.5 ± 6.4 (6.9 %)	**110.7 ± 14.9 (50 %)**	164.3 ± 11.9 (43.1 %)

[a]P1, P2, and P3 are the best fit peak ages extracted from the age populations using binomial peak fitting as described in *Stewart and Brandon* [2004], with the percentage of single-grain ages making up the peak in parentheses. The main age population is shown in bold.
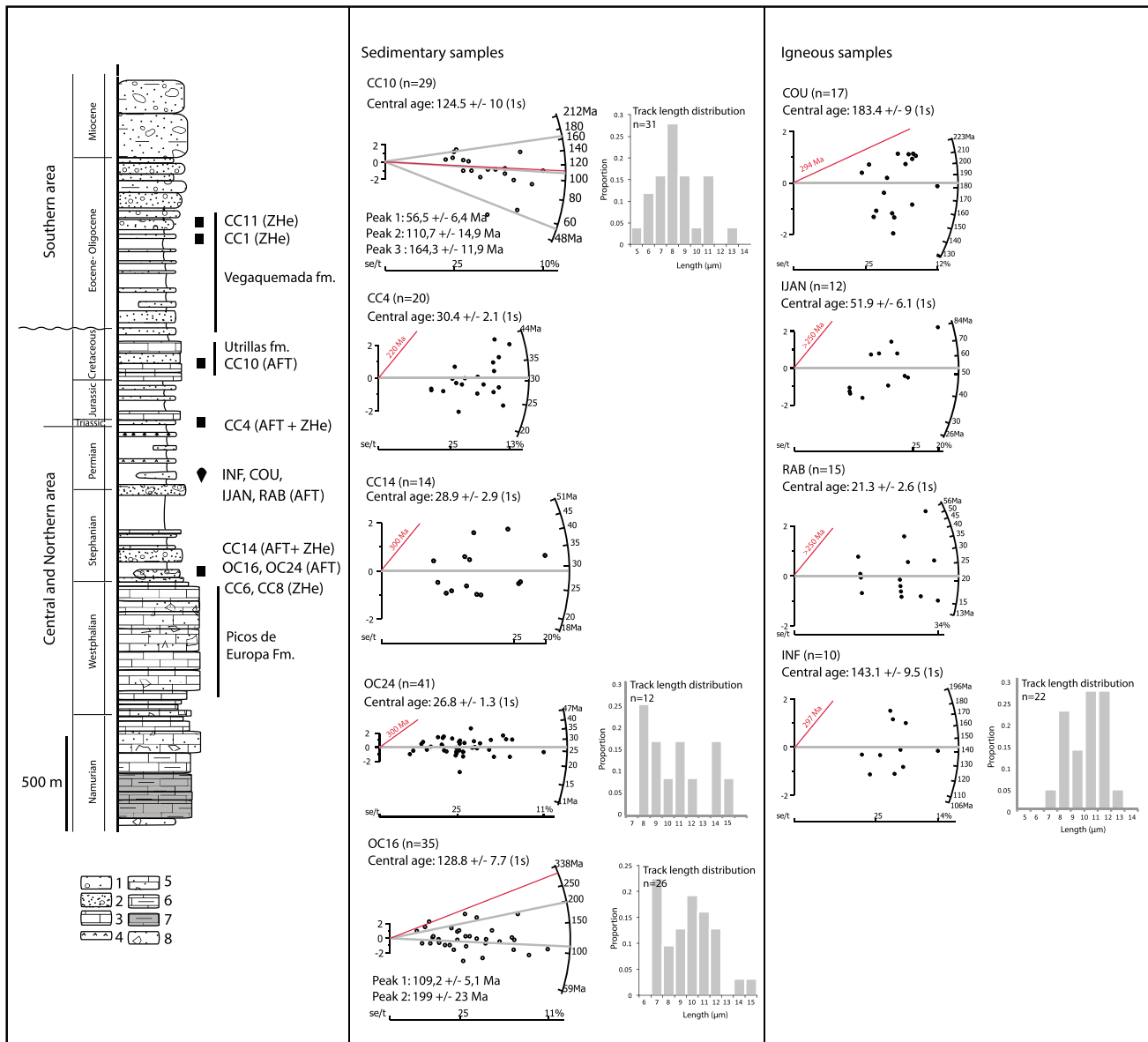
Figure 3. Grain age populations (shown as radial plots), track length measurements when available, and stratigraphic positions of the samples. Depositional ages are indicated by red lines in the radial plots. Samples COU, IJAN, RAB, and INF come from Grabboic or granodiorite rocks; the age represented is therefore the crystallization age. Samples CC10 and OC16 are partially reset and present three and two populations of AFT ages, respectively. The other samples are all fully reset. To the left is a synthetic stratigraphic column with sample positions, modified after *Garcia-Ramos and Gutierrez-Claverol* [1995], *Alonso et al.* [1996], *Gomez-Fernandez et al.* [2000], and *Herrero et al.* [2010]. Keys: 1. Conglomerates; 2. Sandstones; 3. Limestones; 4. Volcanoclastics; 5. Rudstones with breccias; 6. Mudstones; 7. Black-laminated limestones; and 8. Nodular limestones.

indicate that both samples have grains with inherited thermal histories and both have been partially reset since deposition. Measured track lengths are very short in both cases, with a mean track length of $9.0 \pm 0.4\,\mu m$ for OC16 ($n = 26$) and $10.1 \pm 0.4\,\mu m$ for CC10 ($n = 31$), indicating that the samples resided a long time in the partial annealing zone (PAZ).

4.2. Western Samples

Despite the large amount of samples collected in the western profile, only one of them, in the center of the Central Coal Basin (OC24), allowed us to obtain an AFT age. Two more samples of small basic igneous outcrops of Permian age yielded sufficient apatite: one close to the Oviedo basin to the northeast of OC24 (sample INF) and one to the northwest (sample COU). Of these three samples, only OC24 clearly records
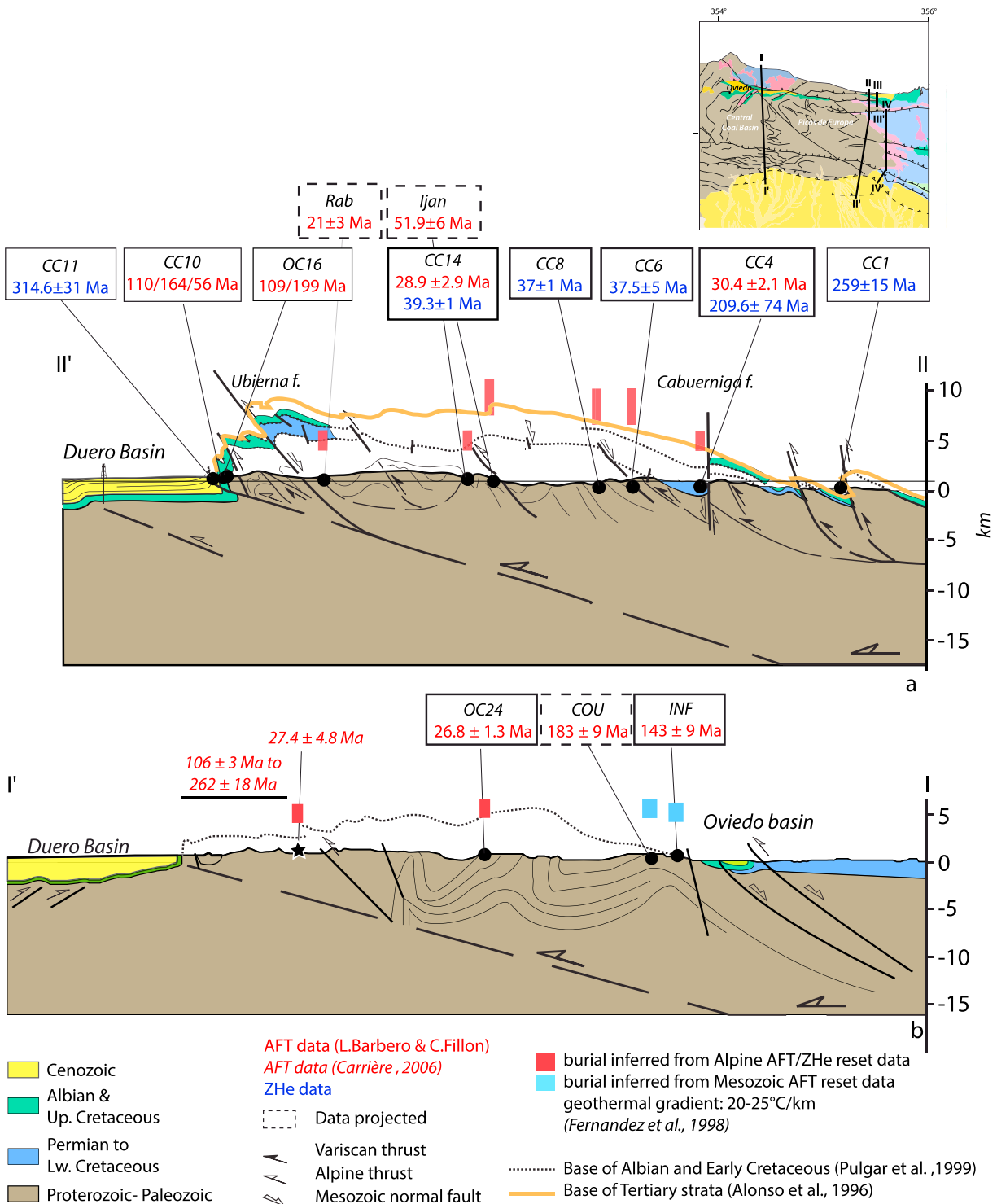
Figure 4. North-south cross sections located in the central Cantabrian Mountains (top: section II-II′ near the border with the Basque-Cantabrian basin; bottom: section I-I′ some ~70 km to the west, crossing the carboniferous Central Coal Basin), with projected ages from this study and *Carrière* [2006]. AFT ages are in red and ZHe ages in blue. Structural cross sections are redrawn from *Pulgar et al.* [1999]. Sample locations (black dots) were projected onto the section at their corresponding heights, following the structural trends. The red bars represent the projection of the inferred ZHe PRZ (160–200°C) for samples CC6, CC8, and CC14 and of the AFT PAZ (100–120°C) for CC4. They represent the minimum burial required to obtain the observed ZHe and AFT ages and therefore mark the minimum estimated top of Mesozoic sediments. This is compared to the base of the Tertiary strata inferred from the structural study of *Alonso et al.* [1996] (orange line). The blue bars represent the same burial estimation but for the reset AFT samples during Mesozoic times.
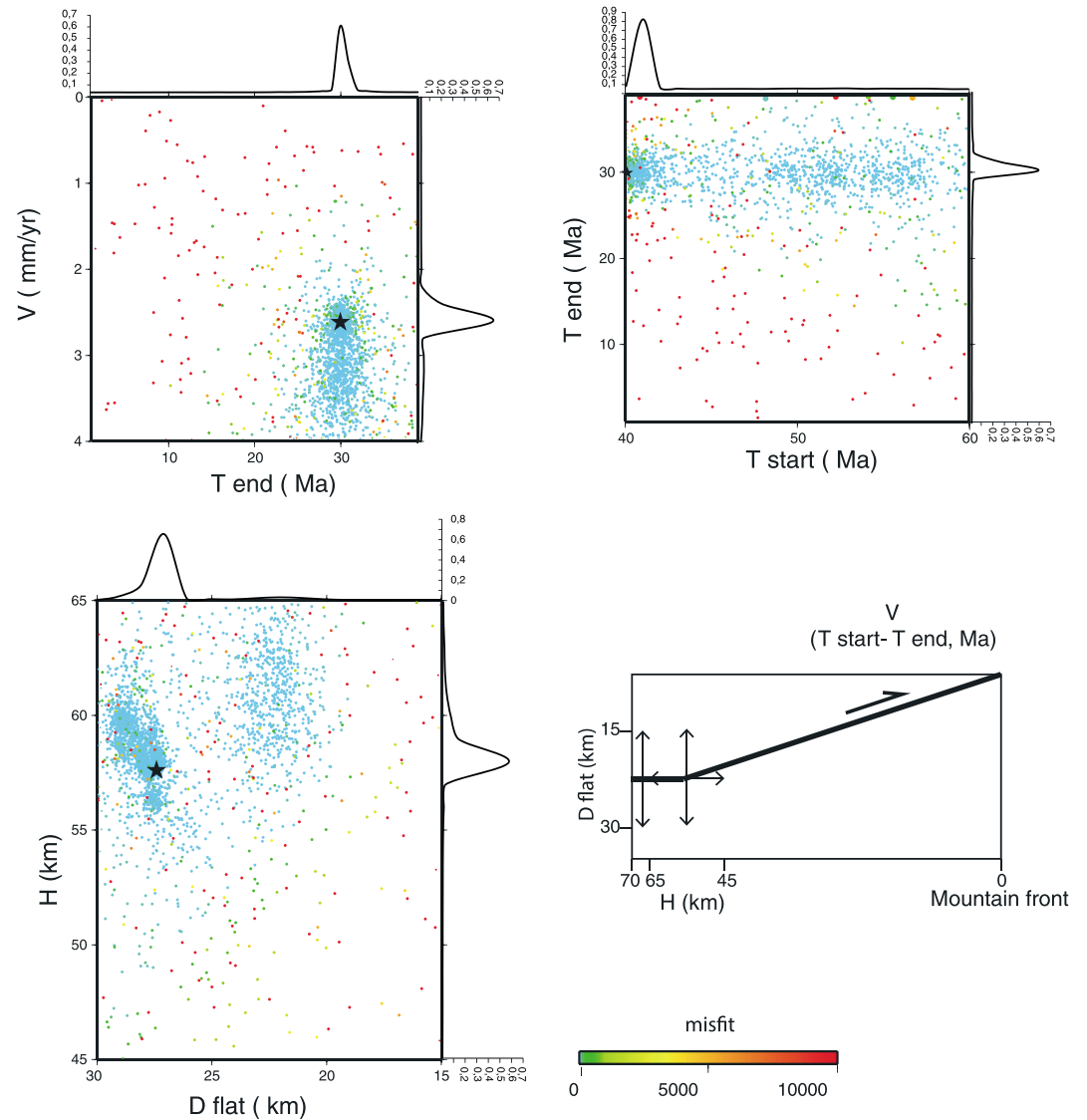
Figure 5. Inversion results from 3-D thermokinematic modeling using *Pecube*. plots represent the distribution in the 2-D parameter space of the model results, colored according to their misfit. Black stars mark the overall best fit solution. Curves along the axes are the 1-D posterior probability density functions for the values of each parameter tested. (bottom right) Sketch illustrating the geometry of the crustal structure and the structural kinematic parameters tested.

Oligocene exhumation, with an age of 26.8 ± 1.3 Ma, consistent with the AFT results presented previously and an Oligocene AFT age of 27.4 ± 4.8 Ma obtained further south by *Carrière* [2006] (white star in Figures 2 and 4). The two other samples to the north show resetting during Early Jurassic and Early Cretaceous times, with single-population AFT ages of 183 ± 9 Ma (COU) and 143 ± 9 Ma (INF), respectively. Note that the lack of Cenozoic resetting in the north is consistent with the decrease in the amount of exhumation deduced from the cross sections and observed also in the northern part of the eastern transect.

4.3. Three-Dimensional Thermokinematic Modeling

To extract a more general pattern of exhumation rates and timing from our data set, we present here inverse modeling results for the central Cantabrian samples. We use a 3-D thermokinematic model (Pecube, *Braun* [2003], and *Braun et al.* [2012], details on the methods are provided in the supporting information) that allows deriving exhumation histories for a simple prescribed structural-kinematic scenario by inverting the thermochronological data. We base our model on the structural cross section of *Pulgar et al.* [1999] (Figure 4a) in which exhumation in the central Cantabrian Mountains is driven by motion on a major crustal ramp. The
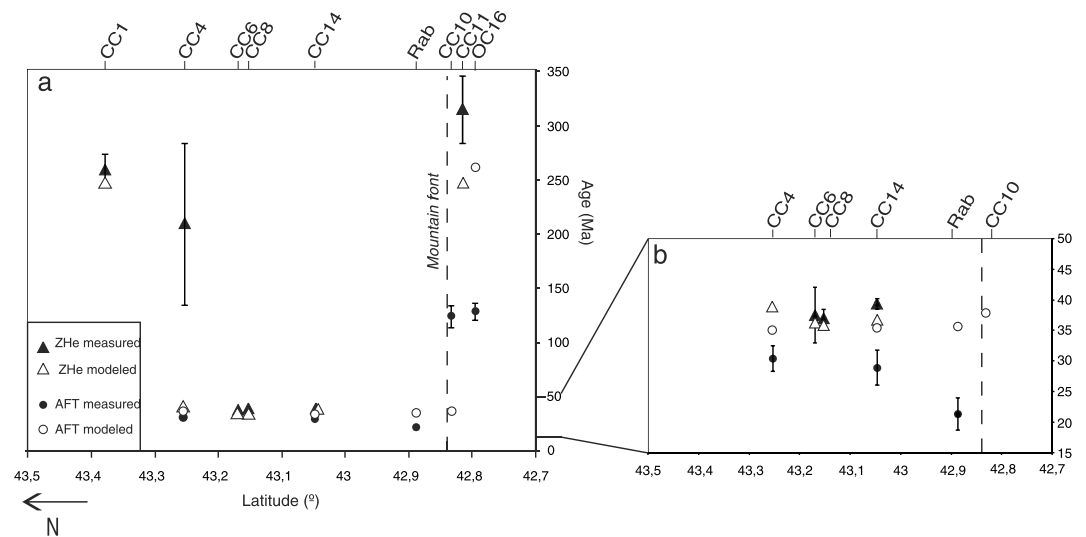
Figure 6. Comparison of predicted and observed AFT and ZHe ages for the optimum model (indicated by black stars in Figure 5). (a) Predicted AFT and ZHe ages (open circles and triangles, respectively) are compared to measured AFT and ZHe data (black circles and triangles). (b) Zoom on the central part of the section and the 15–50 Ma age range.

inverted parameters (see Figure 5) are the velocity along the frontal ramp (V, varying from 0 to 4 mm yr^{-1}), the starting and ending times of the main exhumation phase ($Tstart$ and $Tend$, varying from 60 to 40 Ma and from 39 to 1 Ma, respectively), the horizontal distance between the front of the ramp and the inflection point between the ramp and the flat (H, varying from 45 to 65 km), and the depth of the flat (D flat, varying from 15 to 30 km). The latter two parameters allow varying the ramp geometry [e.g., *Robert et al.*, 2011]. As mentioned in section 2.2, the ramp geometry is constrained on the structural cross section (Figure 4) by the dip of the Mesozoic layers in the dorsal culmination of the crustal fault bend fold, but these layers do not crop out along most of this section, being projected from the east, which introduces some uncertainty. To define the thermal structure, we assume a thermal diffusivity of 25 km^2 Myr^{-1} and an average initial geothermal gradient of 25°C km^{-1}.

The inversion takes into account the central AFT ages of samples CC4, CC14, RAB, CC10, and OC16 (IJAN being too far from the section), together with the track length distribution if any, and the mean ZHe ages of samples CC1, CC4, CC6, CC8, CC14, and CC11. The modeling results show a well-resolved solution with posterior probability density functions of the parameter values defining clear peaks and inversions converging toward consistent values. The best fitting results shown here (black stars in Figure 5) place the base of the ramp at ~58 km of horizontal distance from the front, associated with a depth of 27 km, giving a ramp angle of 25°. The exhumation phase is defined between 40 Ma and 29.9 Ma and associated to a velocity on the ramp of 2.6 mm yr^{-1}, equivalent to a vertical exhumation rate of 1.1 mm yr^{-1} when considering the angle of the ramp. The fit to the data is good for most of the reset samples (Figure 6), but it is important to note that this model fails to reproduce the AFT age of sample RAB (slightly off the cross section), the partially and unreset samples OC16 and CC10 (located in the forelimb of the frontal fault propagation fold, which is not reproduced in the kinematic model), and the unreset ZHe age of sample CC4. The discussion below attempts to explain these discrepancies. In general, the timing of the exhumation phase (from 40 to 30 Ma) is consistent with the direct interpretation of our results, but the rate of exhumation as well as the structure or the ramp differs from what was expected. The implications of these results will be discussed in the next section.

5. Implications and Discussion

5.1. New Constraints on Timing of Alpine Exhumation in the Central Cantabrians

Our new AFT and ZHe ages allow us to frame the Alpine exhumation of the central Cantabrian Mountains in terms of timing and spatial distribution. The well-reproducible ZHe ages provide a minimum estimate for the onset of Alpine inversion during Bartonian times (39 Ma), which is consistent with the age of the onset of continental sedimentation in the Tertiary Oviedo basin (Bartonian-Priabonian near its base) [*Casanovas-Cladellas et al.*, 1991;
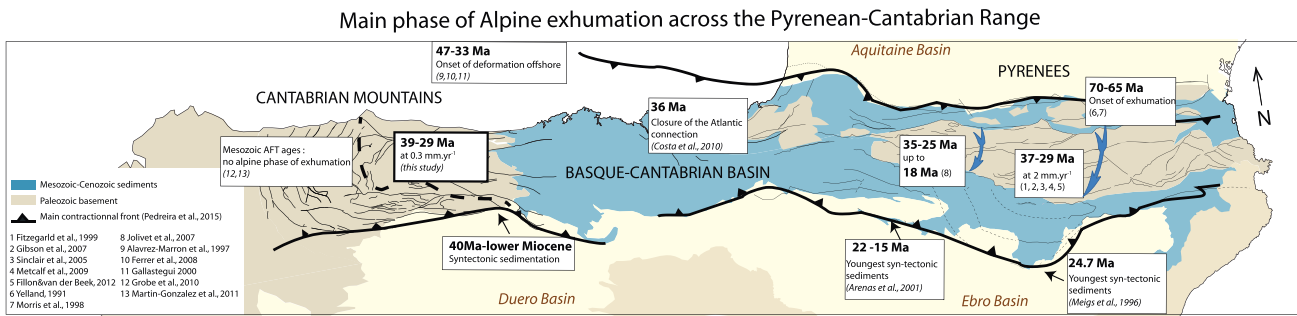
Figure 7. Synthesis map presenting the evidences (and their references in italic) for a synchronous main exhumation phase in the Cantabrian Mountains and in the central Pyrenees from late Eocene to early Oligocene times, including this study. The studies cited here are based on low-temperature thermochronology, magnetostratigraphy of continental sediments, or sedimentological studies.

Truyols and García Ramos, 1991]. This is also consistent with the age of the deformation offshore, dated as middle to late Eocene [*Alvarez-Marron et al.*, 1997; *Ferrer et al.*, 2008; *Gallastegui*, 2000]. The latest potential ending time of this deformation phase is constrained by the youngest AFT ages found along the ESCIN-2 section, which are late Oligocene in age (~30 Ma; results from samples IJAN and RAB will be discussed in a following section). These results are also consistent with the ages of syntectonic sediments outcropping along the northern border of the Duero basin. Although they are not precisely dated, the syntectonic sediments bound the upper limit of frontal thrust activity to late Miocene times, from the age of the sediments unconformably overlying the syntectonic conglomerates. It is also worth noting that the Alpine reset ages do not record any propagation of exhumation from north to south but rather a concentration of exhumation in the center of the section, surrounded by two zones of lesser exhumation to the north and south, where unreset or partially reset ZHe and AFT ages were found.

At a larger scale, our dating also highlight the principal zone of Alpine exhumation in the Cantabrian Mountains area; this signal disappears to the west, as shown by a majority of Mesozoic AFT ages in the western Cantabrians [*Grobe et al.*, 2010; *Martin-Gonzalez et al.*, 2011]. The AFT ages from these two studies range from 53 ± 13 Ma to 212 ± 12 Ma and suggest exhumation rates of 0.05 mm yr^{-1} between 100 and 50 Ma, then 0.02 mm yr^{-1} in the Paleogene and 0.06 mm yr^{-1} in Neogene times [*Grobe et al.*, 2010; *Martin-Gonzalez et al.*, 2011]. To summarize, the combined data set suggest a decrease in the age, amount, and rate of Alpine exhumation from the central to the western Cantabrian Mountains. Further east, there are currently no published AFT data from the Basque-Cantabrian basin area. Within the Pyrenean domain, a major exhumation period is identified in late Eocene-Oligocene times as well. Despite some local complexities, most of the thermochronological studies in the Pyrenees support a main phase of exhumation during late Eocene-Oligocene times at exhumation rates of ~2 mm yr^{-1} [*Fitzgerald et al.*, 1999; *Gibson et al.*, 2007; *Jolivet et al.*, 2007; *Maurel et al.*, 2007; *Metcalf et al.*, 2009; *Morris et al.*, 1998; *Sinclair et al.*, 2005; *Yelland*, 1990]. AFT ages range from 35 to 21 Ma in the Eastern Pyrenees, excluding the northernmost massifs [*Maurel et al.*, 2007; *Morris et al.*, 1998], from 44 to 19 Ma in the central Pyrenees [*Fitzgerald et al.*, 1999; *Sinclair et al.*, 2005], and from 36 to 11 Ma in the western Pyrenees [*Jolivet et al.*, 2007; *Morris et al.*, 1998], with the youngest ages concentrated in the Bielsa Massif (Figure 7). In the south-central Pyrenees, AFT and AHe dating together with thermal modeling of the data [*Fillon and van der Beek*, 2012; *Fitzgerald et al.*, 1999; *Gibson et al.*, 2007; *Metcalf et al.*, 2009; *Sinclair et al.*, 2005; *Rushlow et al.*, 2013] suggest a phase of rapid exhumation between 37 and 29 Ma at a rate of 2.8 ± 0.3 mm yr^{-1}. This time period represents the last phase of convergence of the Pyrenean system and can be followed to the west of the Pyrenees by the uplift of the eastern Basque-Cantabrian basin/western Pyrenees that led to the closure of the Atlantic connection of the Ebro basin, dated at 36 Ma by magnetostratigraphy [*Costa et al.*, 2009]. Therefore, our thermochronological results infer a synchronous main exhumation phase in the Cantabrian Mountains and in the central Pyrenees from late Eocene to early Oligocene times (Figure 7). However, we show from our results that the associated rates are 2–3 times slower in the Cantabrian Mountains as compared to the central Pyrenees.
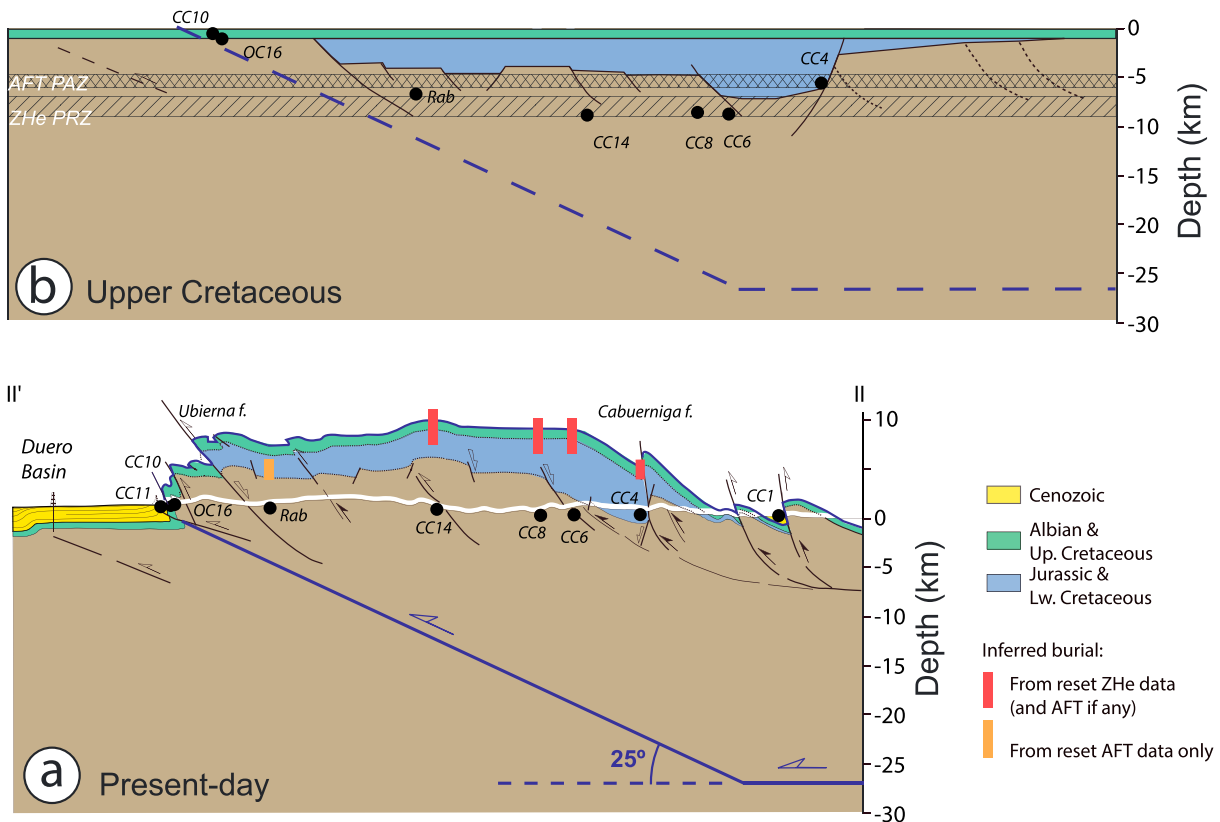
Figure 8. (a) Idealized cartoon showing the uppermost Cretaceous depth distribution of the thermochronological samples, along the section II/II' (Figure 4). Ranges for AFT partial annealing zone (PAZ) and ZHe partial retention zone (PRZ) are represented according to an average geothermal gradient as mentioned in the text. (b) Present-day structural sketch based on the cross section by *Alonso et al.* [1996] and *Pulgar et al.* [1999] and with the geometry of the frontal thrust inferred from the thermokinematic modeling described in section 4.3. Note that the sample IJAN was removed from this sketch because the thickness of the Mesozoic cover is increasing on a short distance to the west, making the projection of this sample incompatible with sample CC14 (see section 5.2).

5.2. Burial Estimates and Structural Implications

5.2.1. Eastern Cross Section

In the central part of the Cantabrian Mountains (Figure 2), the thermochronological ages highlight exhumation patterns that are, to first order, in agreement with the structural interpretation of *Alonso et al.* [1996] and *Pulgar et al.* [1999]. Uplift along a crustal ramp rooted in a horizontal detachment induces maximum and synchronous uplift above the shallower part of the ramp, bounded by two zones of less exhumation to the back (dorsal culmination of the fault bend fold) and front (fault propagation fold). Unreset ages are encountered in the northern and southern extremities of the range, and the reset samples are located in the center of the section, between the Cabuérniga Fault and the Ubierna Fault (Figure 4a). These two major faults are known to be Mesozoic extensional faults reactivated during Cenozoic contraction [*Pulgar et al.*, 1999]. They both played a major role in the Basque-Cantabrian basin; the Cabuérniga Fault continues to the Picos de Europa unit, whereas the Ubierna Fault extends to the Central Coal Basin area, where it is named Leon Fault.

The reset ages allow us to estimate a minimum amount of pre-Alpine burial for these samples, depending on the assumed geothermal gradient. The present-day geothermal gradient in the area is ~20°C/km [*Fernàndez et al.*, 1998], but it is reasonable to assume it could have been slightly higher at the onset of Alpine contractional deformation. Considering the range between 20 and 25°C/km, and a surface temperature of 0°C, the upper boundary of the ZHe partial retention zone (PRZ) (~160°C) would be encountered at 6.4 to 8 km depth, while the lower surface (~200°C) would be at 8 to 10 km. When projecting on top of each sample the amount of preorogenic burial needed to reset the AFT and ZHe systems, we observe a fairly good agreement with the structural interpretation of *Alonso et al.* [1996] and *Pulgar et al.* [1999], when considering the upper surface of the PAZ and PRZ (Figure 4a). The main discrepancies occur for samples CC6, CC8, and CC14 in the center of

the range, which require up to ~3 km of additional sedimentary cover with respect to the earlier structural interpretation, if we consider the lower surface of the PRZ and the colder geothermal gradient. We should add here again a cautionary note about the reset thermochronometric ages of sample CC4 because this sample is located at ~300 m to the south of the Cabuérniga thrust, which focuses hydrothermal activity even at present. Also, some amount of tectonic burial by the south directed Cabuérniga thrust is to be expected before this structure rotated to a subvertical position by the monoclinal flexure induced by the flat-ramp geometry of the frontal thrust. Hence, some heating of the sample (potentially leading to older ZHe ages) probably occurred by processes that cannot be simulated in the kinematic model. In any case, assuming that all the burial was sedimentary, the elevated horizontal surface above the ramp must be extended some ~10 km to the north to fit the data. This would also imply increasing the dip of the "dorsal culmination" [*Butler*, 1982] of the fault bend fold and therefore the dip and maximum depth of the ramp. We note that *Alonso et al.* [1996] constrained the top of the Mesozoic in the dorsal culmination by prolonging the dip of the layers in the northern part of the section and projecting them from the east of the section (see orange line in Figure 4a), which obviously introduces some uncertainties. In fact, the results of the ESCIN-2 seismic reflection profile, published after this model was proposed, provided a good image of this ramp in which its dip angle is interpreted to be higher than originally proposed [*Gallastegui*, 2000; *Pulgar et al.*, 1997]. This is also consistent with the results of our 3-D kinematic modeling.

Our thermochronological results lead to a reconstructed Mesozoic cover with a maximum thickness between ~4–6 km and ~6.4–10 km (Figure 8, constrained by AFT and ZHe reset ages, respectively, with an AFT PAZ between 100 and 120°C, a ZHe PRZ of 160–200°C, and assuming a geothermal gradient of 20 to 25°C/km) immediately to the south of the Cabuérniga Fault (Figure 4a).

In terms of exhumation rates, the best estimate is provided by sample CC14, for which both the AFT and ZHe thermochronometers were reset in Cenozoic times. These two ages in sample CC14 indicate that it took ~10 Myr (39 Ma to 29 Ma) for the sample to be exhumed from the top of the ZHe PRZ (~160°C) to the top of the AFT PAZ (~100°C). Based on the range of thermal gradients considered (20–25°C/km), sample CC14 provides an estimated exhumation rate of 0.24–0.3 km Myr^{-1} from middle Eocene to early Oligocene times. This estimate of exhumation rate is significantly smaller than that of 1.1 km Myr^{-1} estimated from the thermokinematic modeling; this discrepancy will be discussed below.

5.2.2. Western Cross Section

Due to the lack of suitable samples, exhumation patterns along the western cross section are much less constrained. Our single AFT age in the center of the Central Coal Basin (OC24) suggests burial of 4 to 6 km (with an AFT PAZ between 100 and 120°C and assuming a geothermal gradient of 20 to 25°C/km), which is consistent with the projected top of the Mesozoic sediments inferred by *Alonso et al.* [1996] and *Pulgar et al.* [1999], considering the uncertainties in both methods of burial estimates (Figure 4b). The AFT ages produced by *Carrière* [2006] are also in agreement with the published structure, as he reports an Oligocene AFT age 10 km to the south of our sample and unreset ages further to the south, where the amount of Alpine exhumation is supposed to be less.

To the North, Alpine exhumation is also less significant, as evidenced by the preservation of Tertiary rocks in the Oviedo Basin (Figure 4b). This observation is supported by our AFT data that indicate resetting well before the Alpine phase, during Jurassic to early Cretaceous times, implying that burial never exceeded 4–6 km since Mesozoic times in that area.

5.2.3. Samples IJAN and RAB

Two AFT ages are not in total agreement with the other data, showing either older (IJAN; 52 ± 6 Ma) or younger (RAB; 21 ± 3 Ma) AFT ages. Both these samples were collected east of the ESCIN-2 profile, at the limit between the central Cantabrian Mountains and the Basque-Cantabrian basin (see Figure 2). Figure 4a shows the position of the samples projected along the central cross section and showing that these two samples are both located in the vicinity of major thrusts. Their burial/exhumation history could have thus been perturbed by local structural variations. The Rabanal sample is located in the hanging wall of the inverted Ubierna Fault and could have recorded additional local exhumation related to this fault. This interpretation is consistent with the identification of Miocene transpressional/contractional activity in the Ubierna Fault and the band between this structure and the mountain front [*Carola et al.*, 2015], as well as with the lower-middle Miocene age (pre-Vallesian) inferred for conglomeratic deposits with spectacular growth strata geometries outcropping in the northern Duero basin [*Herrero et al.*, 2010]. The IJAN sample is located even further east at the transition with the Basque-Cantabrian basin (Figure 2)

and could have recorded less exhumation. The sample fails the χ^2 test and shows high age dispersion (23%); it has therefore only been partially reset during Cenozoic times (post-52 Ma).

5.3. Three-Dimensional Thermal Modeling

Modeling of the data provides interesting results but is limited by the amount of thermochronological data along the section. Nevertheless, it is a starting point to discuss the timing and rates of exhumation inferred by the direct interpretation of the data, as well as the structure involved in the deformation of the central Cantabrians. In terms of structure, one important difference between the simplified kinematic model and the real geological structure is that the model thrust plane reaches the surface, whereas in the geological section the thrust motion is accommodated at uppermost crustal levels by a fault propagation fold. This means that the model overpredicts the gradient of exhumation for the samples located at the very front of the range (e.g., CC10, CC11, and OC16; Figure 6a), and therefore, a good fit to these data is not to be expected. Moreover, the model predicts significantly higher exhumation rates (1.1 km Myr^{-1}) than what was inferred by sample CC14 (0.24–0.3 km Myr^{-1}). This difference arises from the fact that the model aims at integrating all the data together and finds an optimum solution to fit a majority of the data (see Figure 6), giving most weight to the reset ZHe ages because they have the smallest uncertainties, which enter in the calculation of the fit (cf. supporting information). In detail, Figure 6b shows that the average thermochronological age of the reset samples is modeled but not the small variations in age from one sample to another. Therefore, the model predicts AFT and ZHe ages that are all in the range 35–40 Ma, leading to more rapid exhumation than inferred directly from the data. However, the start and end times for the modeled exhumation phase fit very well with what was expected from our data. Finally, in terms of geometry, the reference structure as drawn by *Pulgar et al.* [1999] included a ramp dipping at 18° and rooting at 17–18 km depth, while the revised version of *Gallastegui* [2000] based on the ESCIN-2 profile considered a ramp angle of 36°. To reproduce our data set, our model infers a ramp rooting at 27 km with a dip angle of 25°. Therefore, our model is consistent with the structural cross sections of *Pulgar et al.* [1999] and *Gallastegui* [2000]. We note, however, that the limited data set at the surface is probably insufficient to constrain the ramp structure with good resolution [cf. *Robert et al.*, 2011].

6. Conclusions

The combination of apatite fission track analysis and (U-Th)/He measurements on zircons has allowed us to define more precisely the timing and evolution of Alpine exhumation in the central Cantabrian Mountains of northwest Spain. In the eastern part of the studied area, where the Alpine uplift is known to be maximum, the combined AFT and ZHe data provide a precise timing of the onset of exhumation during late Eocene times at the latest (39 Ma), as well as its ending time during the Oligocene (29 Ma), and an average rate of exhumation of 0.24–0.3 km Myr^{-1}. This Alpine exhumation event is synchronous to the main exhumation phase identified in the Pyrenees. The resetting of the ZHe system in samples in the center of the range provides an estimate of the maximum amount of burial experienced by these samples of up to 10 km. In the Central Coal Basin, our three samples are in agreement with the data from *Carrière* [2006], showing Oligocene AFT ages in the center of the section and Mesozoic ages to the north and northwest. The spatial distribution of reset and unreset ages points to localization of exhumation in the center of both sections and does not record any signal of propagation of deformation from north to south, except for a very small band along the mountain front, which seems to show activity until more recent (lower Miocene) times. Thermal modeling of our data set, focused on the central cross section, confirms the time span of the exhumation phase, from 40 to 29 Ma, but predicts a more rapid exhumation rate of 1.1 km Myr^{-1}, illustrating that caution should be exerted in applying inverse thermokinematic modeling to a limited database.

References

Alonso, J. L., J. A. Pulgar, J. C. Garcia-Ramos, and P. Barba (1996), Tertiary basins and Alpine tectonics in the Cantabrian Mountains (NW Spain), in *Tertiary Basins of Spain: The Stratigraphic Record of Crustal Kinematics*, edited by P. F. Friend and C. J. Dabrio, pp. 214–227, Cambridge Univ. Press, New York.

Alvarez-Marron, J., et al. (1996), Seismic structure of the northern continental margin of Spain from ESCIN deep seismic profiles, *Tectonophysics*, *264*, 153–174.

Alvarez-Marron, J., E. Rubio, and M. Torne (1997), Subduction-related structures in the North Iberian Margin, *J. Geophys. Res.*, *102*(B10), 22,497–22,511, doi:10.1029/97JB01425.

Barnolas, A., and V. Pujalte (2004), La Cordillera Pirenaica, in *Geologia de España*, edited by J. Vera, pp. 231–343, SGE-IGME, Madrid.

Boillot, G., J. L. Auxietre, J. P. Dunand, P. A. Dupeuble, and A. Mauffret (1979), The northwestern Iberian margin: A Cretaceous passive margin deformed during Eocene, in *Deep Drilling Results in the Atlantic Ocean: Continental Margins and Paleoenvironment*, edited by M. Talwani, W. Hay, and W. B. F. Ryan, pp. 138–153, AGU, Washington, D. C.

Botor, D., and A. A. Anczkiewicz (2015), Thermal history of the Sabero Coalfield (Southern Cantabrian Zone, NW Spain) as revealed by apatite fission track analyses from tonstein horizons: Implications for timing of coalification, *Int. J. Earth Sci.*, *104*, 1779–1793.

Braun, J. (2003), Pecube: A new finite-element code to solve the 3D heat transport equation including the effects of a time-varying finite amplitude surface topography, *Comput. Geosci.*, *29*, 787–794.

Braun, J., P. A. van der Beek, P. Valla, X. Robert, F. Herman, C. Glotzbach, V. Pedersen, C. Perry, T. Simon-Labric, and C. Prigent (2012), Quantifying rates of landscape evolution and tectonic processes by thermochronology and numerical modeling of crustal heat transport using PECUBE, *Tectonophysics*, *524–525*, 1–28.

Butler, R. W. (1982), The terminology of structures in thrust belts, *J. Struct. Geol.*, *4*(3), 239–245.

Carola, E., J. A. Muñoz, and E. Roca (2015), The transition from thick-skinned to thin-skinned tectonics in the Basque-Cantabrian Pyrenees: The Burgalesa Platform and surroundings, *Int. J. Earth Sci.*, 1–25.

Carrière, K. L. (2006), Neoproterozoic to Holocene tectonothermal evolution of the southern Cantabrian Mountains NW Iberia, revealed by apatite fission-track thermochronology, PhD thesis, 289 pp, Rüprecht-Karl Universität Heidelberg, Heidelberg.

Casanovas-Cladellas, M. L., E. Jiménez Fuentes, C. Martín-Closas, S. Moyá-Solá, J. V. Santafé-Llopis, and J. Truyols (1991), Consideraciones sobre la edad del yacimiento Eocénico de Llamaquique (Oviedo, España), *Boletín de Ciencias de la Naturaleza*, I.D.E.A 253–261.

Casas-Sainz, A. M., and G. De Vincente (2009), On the tectonic origin of Iberian topography, *Tectonophysics*, *474*, 214–235.

Choukroune, P., and ECORS Team (1989), The ECORS Pyrenean deep seismic profile reflection data and the overall structure of an orogenic belt, *Tectonics*, *8*, 23–39, doi:10.1029/TC008i001p00023.

Costa, E., M. Garcés, M. López-Blanco, E. Beamud, M. Gómez-Paccard, and J. Cruz Larrasoaña (2009), Closing and continentalization of the South Pyrenean foreland basin (NE Spain): Magnetochronological constrains, *Basin Res.*, *22*(6), 904–917.

Dumitru, T. A. (1993), A new computer-automated microscope stage system for fission-track analysis, *Nucl. Track. Radiat. Meas.*, *21*(4), 575–580.

ECORS Pyrenees Team (1988), The ECORS deep seismic profile reflection survey across the Pyrenees, *Nature*, *331*, 508–811.

Espina, R. G., G. De Vicente, and A. Muñoz Martin (1996), Analisis poblacional de fallas alpinas en el borde occidental de la Cuenca Vasco-Cantabrica (Cordillera Cantabrica, NO de España), *Geogaceta*, *20*(4), 936–938.

Espina, R. G., J. L. Alonso, and J. A. Pulgar (2004), Extensión Triásica en la Cuenca Vasco-Cántabrica, *Geología de España. SGE-IGME*, Madrid, 338–339.

Farley, K. A., R. A. Wolf, and L. T. Silver (1996), The effects of long alpha-stopping distances on (U---Th)/He ages, *Geochim. Cosmochim. Acta*, *60*(21), 4223–4229.

Fernàndez, M., I. Marzán, A. Correia, and E. Ramalho (1998), Heat flow, heat production, and lithospheric thermal regime in the Iberian Peninsula, *Tectonophysics*, *291*(1–4), 29–53.

Fernández-Viejo, G., J. Gallart, J. A. Pulgar, J. J. Dañobeitia, and D. Córdoba (1998), Crustal transition between continental and oceanic domains along the North Iberian Margin from wide angle seismic and gravity data, *Geophys. Res. Lett.*, *25*(23), 4249–4252, doi:10.1029/1998GL900149.

Fernández-Viejo, G., J. Gallart, J. A. Pulgar, D. Córdoba, and J. J. Dañobeitia (2000), Seismic signature of Variscan and Alpine tectonics in NW Iberia: Crustal structure of the Cantabrian Mountains and Duero basin, *J. Geophys. Res.*, *105*(B2), 3001–3018, doi:10.1029/1999JB900321.

Fernández-Viejo, G., J. A. Pulgar, J. Gallastegui, and L. Quintana (2012), The fossil accretionary wedge of the Bay of Biscay: Critical wedge analysis on depth-migrated seismic sections and geodynamical implications, *J. Geol.*, *120*(3), 315–331.

Ferrer, O., E. Roca, B. Benjumea, J. A. Muñoz, N. Ellouz, and M. Team (2008), The deep seismic reflection MARCONI-3 profile: Role of extensional mesozoic structure during the Pyrenean contractional deformation at the eastern part of the Bay of Biscay, *Mar. Pet. Geol.*, *25*, 714–730.

Fillon, C., and P. van der Beek (2012), Post-orogenic evolution of the southern Pyrenees: Constraints from inverse thermo-kinematic modelling of low-temperature thermochronology data, *Basin Res.*, *24*(4), 418–436.

Fitzgerald, P. G., J. A. Muñoz, P. J. Coney, and S. L. Baldwin (1999), Asymmetric exhumation across the Pyrenean orogen: Implications for the tectonic evolution of a collisional orogen, *Earth Planet. Sci. Lett.*, *173*, 157–170.

Galbraith, R. F., and G. M. Laslett (1993), Statistical models for mixed fission track ages, *Nucl. Track. Radiat. Meas.*, *21*(4), 459–470.

Galbraith, R. F., and P. F. Green (1990), Estimating the component ages in a finite mixture, *Nucl. Track. Radiat. Meas.*, *17*(3), 197–206.

Gallastegui, J. (2000), Estructura cortical de la cordillera y margen continental cantabricos: Perfiles ESCI-N, *Trab. Geol.*, *22*, 234.

Gallastegui, J., J. Pulgar, and J. Gallart (2002), Initiation of an active margin at the North Iberian continent-ocean transition, *Tectonics*, *21*(4), 1033, doi:10.1029/2001TC901046.

Garcia-Ramos, J. C., and M. Gutierrez-Claverol (1995), La cobertera Mesozoico-Terciaria, Geologia de Asturias, edited by C. Aramburu, F. Bastida, pp. 81–94, Trea, Gijon.

Gibson, M., H. D. Sinclair, G. J. Lynn, and F. M. Stuart (2007), Late- to post-orogenic exhumation of the Central Pyrenees revealed through combined thermochronological data and modelling, *Basin Res.*, *19*(3), 323–334.

Gomez-Fernandez, F., R. A. Both, J. Mangas, and A. Arribas (2000), Metallogenesis of Zn-Pb carbonate-hosted mineralization in the southeastern region of the picos de europa (Central Northern Spain) province: Geologic, fluid inclusion, and stable isotope studies, *Econ. Geol.*, *95*(1),19–40.

Grobe, R. W., J. Alvarez-Marrón, U. A. Glasmacher, and R. Menéndez-Duarte (2010), Low-temperature exhumation history of Variscan-age rocks in the western Cantabrian Mountains (NW Spain) recorded by apatite fission-track data, *Tectonophysics*, *489*(1–4), 76–90.

Gunnel, Y., M. Calvet, S. Brichau, A. Carter, J.-P. Aguilar, and H. Zeyen (2009), Low long-term erosion rates in high-energy mountain belts: Insights from thermo- and biochronology in the Eastern Pyrenees, *Earth Planet. Sci. Lett.*, *278*(3–4), 208–218.

Herrero, A., G. Alonso-Gavilán, and J. R. Colmenero (2010), Depositional sequences in a foreland basin (north-western domain of the continental Duero basin, Spain), *Sediment. Geol.*, *223*, 235–264.

Herrero-Hernández, A., and F. Gómez-Fernández (2012), Palaeoshoreline for the Late Cretaceous marine platform in the Iberian Trough (Leonese Area, Spain) deduced from outcrop and subsurface analysis, *Open Geosci.*, *4*(3), 395–415.

Hurford, A. J., and P. F. Green (1983), The zeta age calibration of fission-track dating, *Chem. Geol.*, *41*, 285–317.

Julivert, M. (1971), Decollement tectonics in the Hercynian Cordillera of Northwest Spain, *Am. J. Sci.*, *270*(1), 1–29.

Jolivet, M., P. Labaume, P. Monié, M. Brunel, N. Arnaud, and M. Campani (2007), Thermochronology constraints for the propagation sequence of the south Pyrenean basement thrust system (France-Spain), *Tectonics*, *26*, TC5007, doi:10.1029/2006TC002080.

Lepvrier, C., and E. Martinez-Garcia (1990), Fault development and stress evolution of the post-Hercynian Asturian Basin (Asturias and Cantabria, northwestern Spain), *Tectonophysics*, *184*(3–4), 345–356.

Martin-Gonzalez, F., and N. Heredia (2011), Complex tectonic and tectonostratigraphic evolution of an Alpine foreland basin: The western Duero Basin and the related Tertiary depressions of the NW Iberian Peninsula, *Tectonophysics*, *502*(1–2), 75–89.

Martin-Gonzalez, F., L. Barbero, R. Capote, N. Heredia, and G. Gallastegui (2011), Interaction of two successive Alpine deformation fronts: Constraints from low-temperature thermochronology and structural mapping (NW Iberian Peninsula), *Int. J. Earth Sci.*, 1–12.

Maurel, O., P. Moniè, R. Pik, N. Arnaud, M. Brunel, and M. Jolivet (2007), The Meso-Cenozoic thermo-tectonic evolution of the Eastern Pyrenees: An Ar/Ar fission track and (U-Th)/He thermochronological study of the Canigou and Mont-Louis massifs, *Int. J. Earth Sci.*, *97*, 565–584.

Meigs, A. J., J. Verges, and D. W. Burbank (1996), Ten-million-year history of a thrust sheet, *Geol. Soc. Am. Bull.*, *108*(12), 1608–1625.

Metcalf, J. R., P. G. Fitzgerald, S. L. Baldwin, and J. A. Muñoz (2009), Thermochronology of a convergent orogen: Constraints on the timing of thrust faulting and subsequent exhumation of the Maladeta Pluton in the Central Pyrenean Axial Zone, *Earth Planet. Sci. Lett.*, *287*(3–4), 488–503.

Morris, R. G., H. D. Sinclair, and A. J. Yelland (1998), Exhumation of the Pyrenean orogen: Implications for sediment discharge, *Basin Res.*, *10*, 69–86.

Mouthereau, F., P. Y. Filleaudeau, A. Vacherat, R. Pik, O. Lacombe, M. G. Fellin, S. Casteltort, F. Christophoul, and E. Masini (2014), Placing limits to shortening evolution in the Pyrenees: Role of margin architecture and implications for the Iberia/Europe convergence, *Tectonics*, *33*, 2283–2314, doi:10.1002/2014TC003663.

Muñoz, J. A. (1992), Evolution of a continental collision belt: ECORS Pyrenees crustal balanced cross section, in *Thrust Tectonics*, edited by K. R. McClay, pp. 235–246, Chapman & Hall, London.

Olivet, J.-L. (1996), La cinématique de la plaque Ibérique, *Bull. Cent. Rech. Explor. Prod. Elf Aquitaine*, *20*, 131–195.

Pedreira, D., J. A. Pulgar, J. Gallart, and J. Diaz (2003), Seismic evidence of Alpine crustal thickening and wedging from the western Pyrenees to the Cantabrian Mountains (north Iberia), *J. Geophys. Res.*, *108*(B4), 2204, doi:10.1029/2001JB001667.

Pedreira, D., J. A. Pulgar, J. Gallart, and M. Torné (2007), Three-dimensional gravity and magnetic modeling of crustal indentation and wedging in the western Pyrenees-Cantabrian Mountains, *J. Geophys. Res.*, *112*, B12405, doi:10.1029/2007JB005021.

Pedreira, D., J. C. Afonso, J. A. Pulgar, J. Gallastegui, A. Carballo, M. Fernàndez, D. García-Castellanos, I. Jiménez-Munt, J. Semprich, and O. García-Moreno (2015), Geophysical-petrological modeling of the lithosphere beneath the Cantabrian Mountains and North-Iberian margin: geodynamic implications, *Lithos*, *230*, 46–48.

Pérez-Estaùn, A., F. Bastzda, J. L. Alonso, J. Marqufnez, J. Aller, J. Alvarez-Marron, A. Marcos, and J. A. Pulgar (1988), A thin-skinned tectonics model for an arcuate fold and thrust belt: The cantabrian zone (Variscan Ibero-Armorican Arc), *Tectonics*, *7*(3), 517–537, doi:10.1029/TC007i003p00517.

Pujalte, V., S. Robles, J. García-Ramos, and J. Hernández (2004), El Malm-Barremiense no marinos de la Cordillera Cantábrica, *Geología de España*. SGE-IGME, Madrid, 288–291.

Pulgar, J. A., J. Gallart, G. Fernandez-Viejo, A. Perez-Estaun, J. Alvarez-Marron, and E. Group (1996), Seismic image of the Cantabrian Mountains in the western extension of the Pyrenees from integrated ESCIN reflection and refraction data, *Tectonophysics*, *264*(1–4), 1–19.

Pulgar, J. A., J. Pérez-Estaùn, J. Gallart, J. Alvarez-Marron, J. Gallastegui, J. L. Alonso, and E. Group (1997), The ESCI-N2 deep seismic reflection profile: A traverse across the Cantabrian Mountains and adjacent Duero basin, *Rev. Soc. Geol. Esp.*, *8*(4), 383–394.

Pulgar, J. A., J. L. Alonso, R. G. Espina, and J. A. Marín (1999), La deformación alpina en el basamento varisco de la Zona Cantábrica, *Trab. Geol. Univ. Oviedo*, *21*, 283–294.

Robert, X., P. Van Der Beek, J. Braun, C. Perry, and J. L. Mugnier (2011), Control of detachment geometry on lateral variations in exhumation rates in the Himalaya: Insights from low-temperature thermochronology and numerical modeling, *J. Geophys. Res.*, *116*, B05202, doi:10.1029/2010JB007893.

Roca, E., J. A. Muñoz, O. Ferrer, and N. Ellouz (2011), The role of the Bay of Biscay Mesozoic extensional structure in the configuration of the Pyrenean orogen: Constraints from the MARCONI deep seismic reflection survey, *Tectonics*, *30*, TC2001, doi:10.1029/2010TC002735.

Rushlow, C. R., J. B. Barnes, T. A. Ehlers, and J. Vergés (2013), Exhumation of the southern Pyrenean fold-thrust belt (Spain) from orogenic growth to decay, *Tectonics*, *32*, 843–860, doi:10.1002/tect.20030.

Sinclair, H. D., M. Gibson, M. Naylor, and R. G. Morris (2005), Asymmetric growth of the Pyrenees revealed through measurement and modeling of orogenic fluxes, *Am. J. Sci.*, *305*, 369–406.

Stewart, R. J., and M. T. Brandon (2004), Detrital-zircon fission-track ages for the 'Hoh Formation': Implications for late Cenozoic evolution of the Cascadia subduction wedge, *Geol. Soc. Am. Bull.*, *116*(1–2), 60–75.

Teixell, A. (1998), Crustal structure and orogenic material budget in the west central Pyrenees, *Tectonics*, *17*(3), 395–406, doi:10.1029/98TC00561.

Truyols, J., and J. C. García Ramos (1991), El Terciario de la cuenca de Oviedo y el yacimiento de vertebrados de Llamaquique, *Boletín de Ciencias de la Naturaleza*, I.D.E.A 77–99.

Vergés, J., H. Millan, E. Roca, J. A. Muñoz, M. Marzo, J. Cites, T. Den Bezemer, R. Zoetemeijer, and S. Cloetingh (1995), Eastern Pyrenees and related foreland basins: Pre-, syn- and post-collisional crustal-scale cross-sections, *Mar. Pet. Geol.*, *12*(8), 893–915.

Vergés, J., M. Fernàndez, and A. Martínez (2002), The Pyrenean orogen: Pre-, syn-, and post-collisional evolution, *J. Virtual Explor.*, *8*, 57–76.

Weil, A. B., G. Gutiérrez-Alonso, S. Johnston, and D. Pastor-Galán (2013), Kinematic constraints on buckling a lithospheric-scale orocline along the northern margin of Gondwana: A geologic synthesis, *Tectonophysics*, *582*, 25–49.

Yelland, A. J. (1990), Fission track thermotectonics in the Pyrenean orogen, *Nucl. Tracks Radiat. Meas.*, *17*(3), 293–299.

Erratum

In the originally published version of this article, Figure 4 and 8 contained minor errors. These errors have since been corrected, and this version may be considered the authoritative version of record.